

OPTICAL FOLLOW-UP OF GRAVITATIONAL-WAVE EVENTS WITH LAS CUMBRES OBSERVATORY

IAIR ARCAVI^{1,2,12}, CURTIS MCCULLY^{1,2}, GRIFFIN HOSSEINZADEH^{1,2}, D. ANDREW HOWELL^{1,2}, SERGIY VASYLYEV^{1,2},
DOVI POZNANSKI³, MICHAEL ZALTZMAN³, DAN MAOZ³, LEO SINGER^{4,5}, STEFANO VALENTI⁶, DANIEL KASEN^{7,8},
JENNIFER BARNES^{9,12}, TSVI PIRAN¹⁰ AND WEN-FAI FONG^{11,13}¹Department of Physics, University of California, Santa Barbara, CA 93106-9530, USA; arcavi@ucsb.edu²Las Cumbres Observatory, 6740 Cortona Drive, Suite 102, Goleta, CA 93117-5575, USA³Raymond and Beverly Sackler School of Physics and Astronomy, Tel Aviv University, Tel Aviv 69978, Israel⁴Joint Space-Science Institute, University of Maryland, College Park, MD 20742, USA⁵Astrophysics Science Division, NASA Goddard Space Flight Center, Code 661, Greenbelt, MD 20771, USA⁶Department of Physics, University of California, 1 Shields Avenue, Davis, CA 95616-5270, USA⁷Nuclear Science Division, Lawrence Berkeley National Laboratory, Berkeley, CA 94720-8169, USA⁸Departments of Physics and Astronomy, University of California, Berkeley, CA 94720-7300, USA⁹Columbia Astrophysics Laboratory, Columbia University, New York, NY, 10027, USA¹⁰Racah Institute of Physics, The Hebrew University of Jerusalem, Jerusalem 91904, Israel¹¹CIERA and Department of Physics and Astronomy, Northwestern University 2145 Sheridan Road, Evanston, IL 60208, USA¹²Einstein Fellow¹³Hubble Fellow

ABSTRACT

We present an implementation of the [Gehrels et al. \(2016\)](#) galaxy-targeted strategy for gravitational-wave (GW) follow-up using the Las Cumbres Observatory global network of telescopes. We use the Galaxy List for the Advanced Detector Era (GLADE) galaxy catalog, which we show is complete (with respect to a Schechter function) out to ~ 300 Mpc for galaxies brighter than the median Schechter function galaxy luminosity. We use a prioritization algorithm to select the galaxies with the highest chance of containing the counterpart given their luminosity, their position, and their distance relative to a GW localization, and in which we are most likely to detect a counterpart given its expected brightness compared to the limiting magnitude of our telescopes. This algorithm can be easily adapted to any expected transient parameters and telescopes. We implemented this strategy during the second Advanced Detector Observing Run (O2) and followed the black hole merger GW170814 and the neutron star merger GW170817. For the latter, we identified an optical kilonova/macronova counterpart thanks to our algorithm selecting the correct host galaxy fifth in its ranked list among 182 galaxies we identified in the Laser Interferometer Gravitational-wave Observatory LIGO-Virgo localization. This also allowed us to obtain some of the earliest observations of the first optical transient ever triggered by a GW detection (as presented in a companion paper).

Keywords: gravitational waves, methods: observational, galaxies: statistics

1. INTRODUCTION

With the Advanced Laser Interferometer Gravitational-wave Observatory (LIGO; [LIGO Scientific Collaboration et al. 2015](#)) providing detections of gravitational waves (GWs) since 2015 September (e.g. [Abbott et al. 2016a](#)) and with Advanced Virgo ([Acernese et al. 2015](#)) online since 2017 August, it is now feasible to search for electromagnetic (EM) counterparts to GW signals. The main sources of GWs detectable by advanced LIGO/Virgo are mergers of neutron stars and black holes. Of those, neutron star – neutron star (NS–NS) and some neutron star – black hole (NS–BH) mergers are expected to produce

electromagnetic signatures.

In both cases, emission is expected mainly from the radioactive decay of heavy elements formed through the r -process in the merger, as a small amount ($M \sim 10^{-4} - 10^{-2} M_{\odot}$) of neutron-rich material is released at high velocities ($0.1 - 0.3c$) during the final coalescence (e.g. [Rosswog et al. 1999](#); [Rosswog 2005](#); [Hotokezaka et al. 2013](#); [Sekiguchi et al. 2016](#)), and possibly also in outflows from an accretion disk (e.g. [Metzger et al. 2008](#); [Grossman et al. 2014](#); [Kasen et al. 2015](#)). Following the decompression of the ejecta from nuclear densities, rapid neutron capture (r -process) leads to the formation of heavy radioactive elements which then release energy as they decay, powering an electromagnetic light curve

(e.g. Li & Paczyński 1998; Rosswog 2005; Metzger et al. 2010; Goriely et al. 2011; Roberts et al. 2011; Metzger & Berger 2012; Rosswog et al. 2013). These events, which are predicted to be brighter than novae but fainter than supernovae, have been named “macronovae” (Kulkarni 2005) or “kilonovae” (Metzger et al. 2010). Additional emission sources such as free neutron decay leading to prompt blue emission (Metzger et al. 2015) and magnetar spindown (Metzger & Piro 2014) have also been suggested. For recent reviews on kilonovae see Tanaka (2016) and Metzger (2017).

The emission properties of a kilonova depend strongly on the composition of the elements produced in the merger, which is a major source of uncertainty in the models. Heavier elements known as lanthanides can increase the ejecta opacity by several orders of magnitude (Kasen et al. 2013; Tanaka & Hotokezaka 2013), making the light curve fainter, redder, and longer-lived (Barnes & Kasen 2013; Grossman et al. 2014; Wollaeger et al. 2017).

Neutron star mergers are the likely sources also of short gamma-ray bursts (GRBs Eichler et al. 1989; Narayan et al. 1992; Fong & Berger 2013). Excess emission in the afterglows of some short GRBs has been claimed to be due to kilonovae (Perley et al. 2009; Berger et al. 2013; Tanvir et al. 2013; Yang et al. 2015; Jin et al. 2016).

Here we present a search for electromagnetic counterparts to GW events from the second Advanced Detector Observing Run (O2) using the Las Cumbres Observatory global network of telescopes. We describe the observatory and its unique capabilities in §2, our follow-up strategy in §3 and its application to our follow-up of GW170814 (LIGO Scientific Collaboration & Virgo Collaboration 2017a) and GW170817 (LIGO Scientific Collaboration & Virgo Collaboration 2017b,c) in §4. We summarize in §5. Our followup observations of AT 2017gfo, the optical counterpart of GW170817, are described in companion papers (Arcavi et al. 2017a; McCully et al. 2017).

2. LAS CUMBRES OBSERVATORY

Las Cumbres Observatory (LCO)¹ consists of 20 optical telescopes (two 2-meter, nine 1-meter and nine 0.4-meter in diameter) at six sites around the world (Table 1), operated robotically using dynamical scheduling software. The observatory capabilities are described in detail in Brown et al. (2013). Here we summarize the most relevant information.

Table 1. The Las Cumbres Observatory global network of robotic telescopes. Each site is identified by a three-letter airport code for brevity.

Observatory	Location	Code	Telescopes
McDonald	Texas, USA	ELP	1-m ($\times 1$) 0.4-m ($\times 1$)
Haleakala	Hawaii, USA	OGG	2-m ($\times 1$) 0.4-m ($\times 2$)
El Teide	Tenerife, Spain	TFN	0.4-m ($\times 2$)
CTIO	Chile	LSC	1-m ($\times 3$) 0.4-m ($\times 2$)
Siding Spring	Australia	COJ	2-m ($\times 1$) 1-m ($\times 2$) 0.4-m ($\times 2$)
SAAO	South Africa	CPT	1-m ($\times 3$)

Each telescope class uses a different type of imager with a different field of view (FOV) and pixel scale, as listed in Table 2. All imagers are equipped with standard Sloan Digital Sky Survey (SDSS) and Johnson filters, as well as a broad w filter covering the gri bands. The 2-meter telescopes are also equipped with low-resolution ($R \sim 400$) Floyds spectrographs.

Table 2. Imager properties (including fields of view; FOV) for each class of telescope at LCO.

Class	Imager	FOV	Pixel Scale (Binning)
0.4-m	SBIG	$29' \times 19'$	$1.142''/\text{px}$ (2×2)
1-m	Sinistro	$26' \times 26'$	$0.389''/\text{px}$ (1×1)
2-m	Spectral	$10' \times 10'$	$0.3''/\text{px}$ (2×2)

The telescopes are fully robotic and are scheduled by custom software. Users of the observatory submit their requests (which include target information, time constraints, exposure times and the desired telescope class) via web or API² interfaces. Within minutes, the LCO scheduler automatically assigns the requested observations to a telescope, taking into account the observability of the target, the availability of the different telescopes, and the weather conditions at each site. The schedule is re-evaluated approximately every 15 minutes as existing requests are completed, new requests

¹ <http://lco.global/>

² <http://developers.lco.global/>

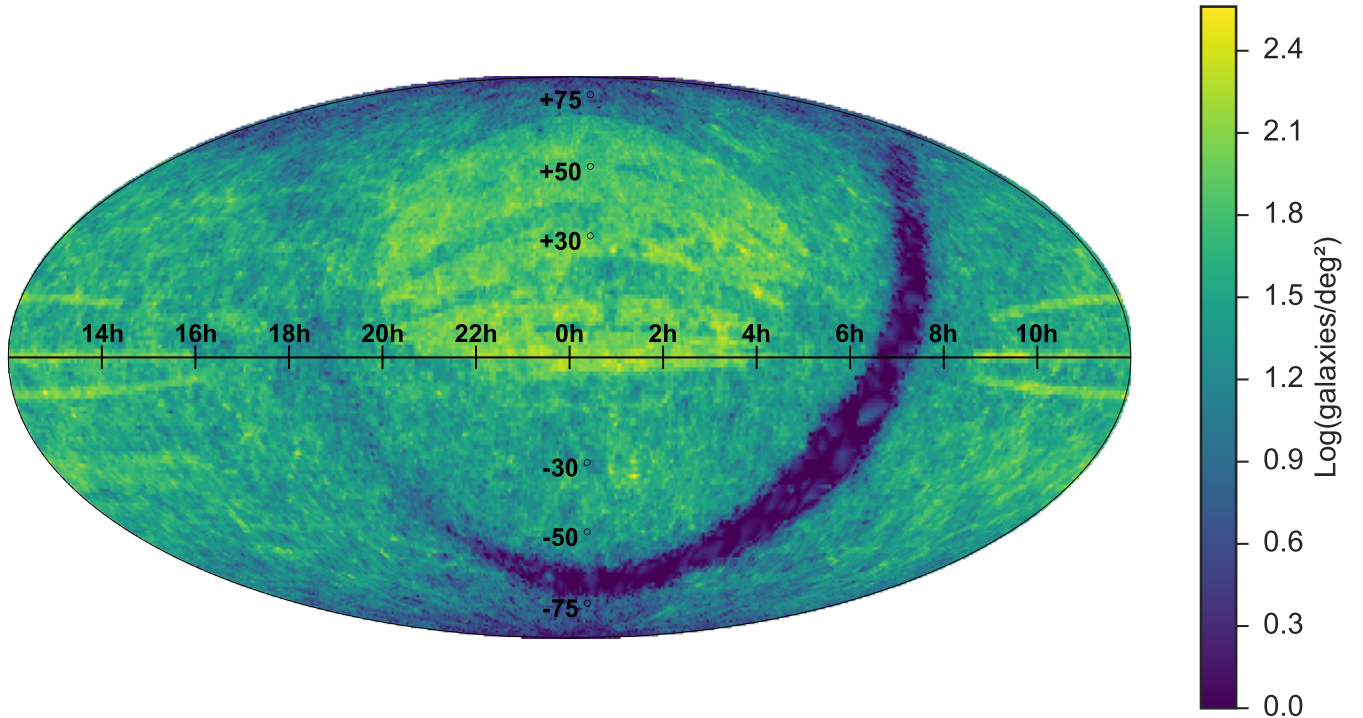


Figure 1. Galaxy density (logarithmically in number of galaxies per square degree) in the GLADE catalog shown in a Mollweide projections of R.A. and decl. The sky coverage, set by the surveys that feed into the GLADE catalog, is clearly not uniform (the low density region follows our Galactic plane). However, with over 1.9 million galaxies with distance and B -band magnitude estimates, GLADE is the most comprehensive publicly available nearby-galaxy catalog as of O2.

are submitted, weather shifts, and telescope availability changes. A special “rapid response” mode, reserved for the most urgent targets, will stop an ongoing observation to observe a new target as soon as possible (shutter opening is typically within a few minutes from the request being submitted - visibility and weather permitting). The dynamic nature of LCO and its global distribution make it ideal for time-domain astronomy, specifically for quick-response observations of rapidly evolving transients.

3. THE FOLLOW-UP STRATEGY

Given the field of view of the LCO imagers, it is not practical to tile an entire GW localization region, which typically ranges in size from tens to hundreds of square degrees (requiring hundreds to thousands of LCO telescope pointings). Instead, we follow the approach presented in [Gehrels et al. \(2016, hereafter G16\)](#), which involves targeting only certain galaxies within the GW localization region.

[G16](#) predicted that the number of galaxies containing 50% of the mass inside a typical O2 GW localization region would be 24 ± 6 (a much more manageable number of pointings compared to tiling the entire localization region). In addition, the Advanced LIGO/Virgo range for mergers involving neutron stars during O2 was ~ 100 Mpc ([Abbott et al. 2016b](#)). At that distance, the

peak observed magnitude of the prompt blue emission from kilonova models is $m_g \sim 21$ ([Metzger et al. 2015](#)) and the peak of the longer optical/near-infrared (NIR) emission is $m_i \sim 19 - 22$ ([Barnes & Kasen 2013](#)). At > 20 Mpc, the smallest LCO field of view corresponds to > 60 kpc thus encapsulating $> 90\%$ of expected merger offsets from their hosts ([Fong & Berger 2013](#)).

These magnitudes, fields of view, and the relatively small number of pointings expected to cover 50% of the mass motivated us to carry out a GW-LCO follow-up program during LCO semesters 2016B and 2017AB, which overlapped with O2.

3.1. The Galaxy Catalog

We use Version 1 of the Galaxy List for the Advanced Detector Era (GLADE; Fig. 1) catalog compiled by [Dalya et al. \(2016\)](#)³. It contains 1,918,147 galaxies amassed from the Gravitational Wave Galaxy Catalog (GWGC [White et al. 2011](#)), the 2MASS XSC ([Skrutskie et al. 2006](#)), the 2MPZ ([Bilicki et al. 2014](#)), and the HyperLEDA ([Makarov et al. 2014](#)) catalogs (Fig. 1). An apparent B -band magnitude is associated with every galaxy from either direct measurement or by deduction from other available magnitudes. GLADE also contains distance information for each galaxy (compiled

³ <http://aquarius.elte.hu/glade/>

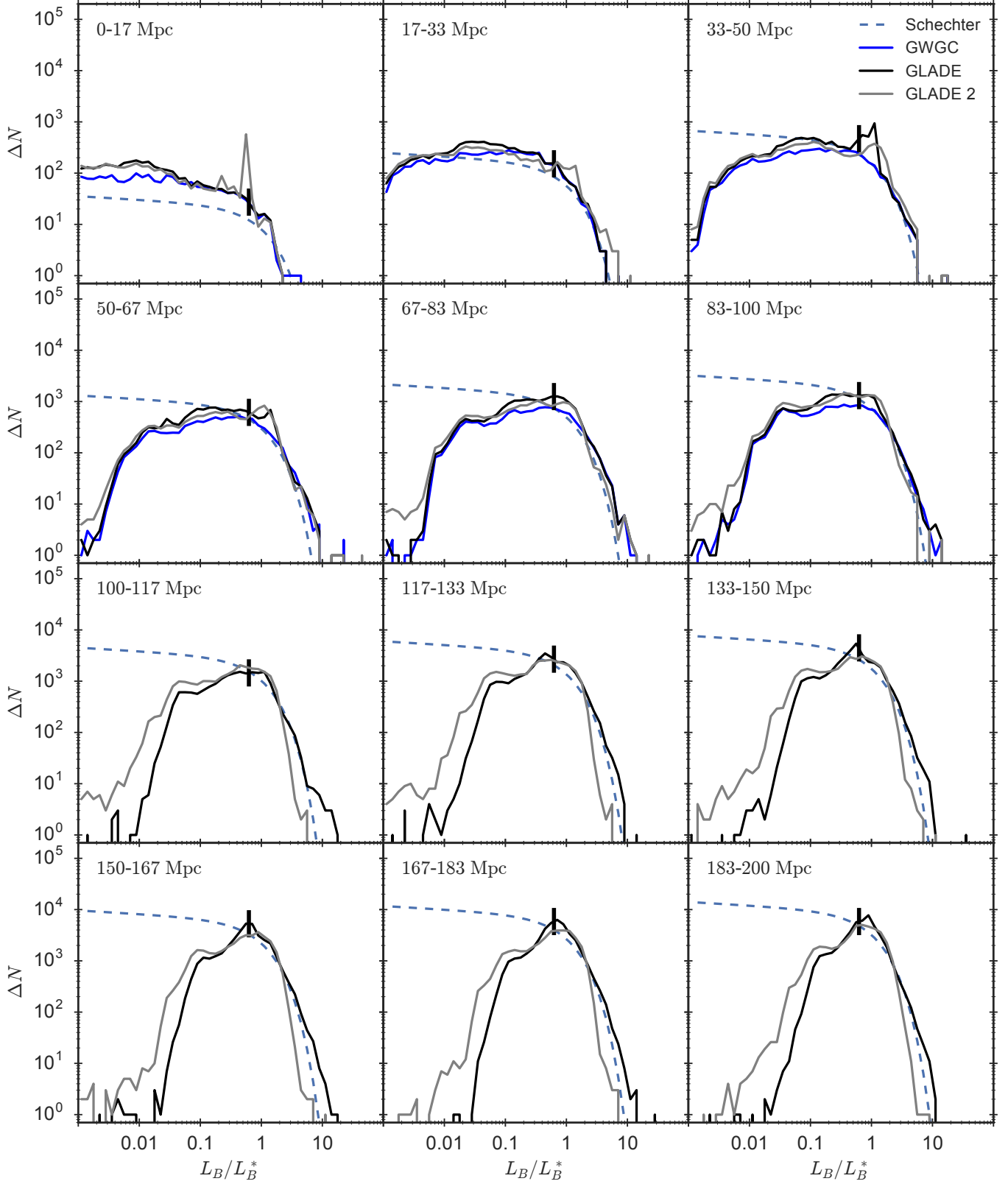


Figure 2. Relative galaxy number density of the GLADE catalogs (version 1 in black, version 2 in gray), the Gravitational Wave Galaxy Catalog (GWGC; blue), and the expected Schechter luminosity function (dashed), corrected for volume, for different distance bins (following G16). $x_{1/2}$ is marked by a vertical line in each plot. Starting at ~ 30 Mpc both GWGC and GLADE miss more and more low-luminosity galaxies; however GLADE is seen to follow the Schechter function quite closely for $L_B/L_B^* > x_{1/2}$ out to 200 Mpc (and beyond, see Figure 3).

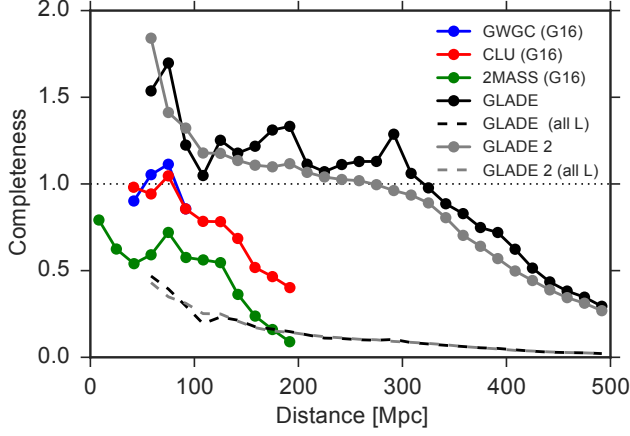


Figure 3. Completeness of GLADE (calculated from Figure 2) relative to the Schechter function for galaxies with $L_B/L_B^* > x_{1/2}$ (i.e. galaxies brighter than the median galaxy luminosity; solid black and gray lines), and for all galaxies (dashed black and gray lines). We also present the data for other catalogs from G16. The greater than 100% completeness for $L_B/L_B^* > x_{1/2}$ galaxies in GLADE at low distances is mostly due to the overabundances of galaxies seen in Figure 2 at these distances. GLADE is complete for $L_B/L_B^* > x_{1/2}$ out to ~ 300 Mpc.

from various sources). Version 2 of the GLADE catalog, containing more than 3.6 million galaxies, was made available during O2. However, compared to Version 1, most of the added galaxies do not have distance or B -band magnitude estimates. We thus chose to continue using Version 1 for the entire O2 run, though we analyze the completeness of both versions below. GLADE is the largest census of the nearby Universe that was publicly available during O2.

Following G16, we analyze the completeness of the GLADE catalog relative to the Schechter luminosity function (Schechter 1976), which provides a form for the number density of galaxies $\rho_{\text{gal}}(x) dx = \phi^* x^\alpha e^{-x} dx$, where $x = L/L^*$ with L the luminosity of the galaxy and L^* a parameter of the function. Since the GLADE catalog contains B -band data, we use $x = L_B/L_B^*$. In order to compare the GLADE catalog with those presented in G16, we adopt the same parameters as they did, namely: $\phi^* = 1.6 \times 10^{-2} h^3 \text{ Mpc}^{-3}$ (with $h = 0.7$), $\alpha = -1.07$ and an L_B^* corresponding to $M_B^* = -20.47$. We reproduce Figure 2 from G16, for the GLADE catalog and the GWGC for comparison, in Fig. 2 here. This figure shows the relative number density of galaxies in GLADE vs. the Schechter function for various distance bins. We also adopt $x_{1/2} = 0.626$ as the median of the luminosity function (i.e. half of the total luminosity is in galaxies above this value and half is in galaxies below it).

While both GWGC and GLADE are missing low-luminosity galaxies at distances greater than ~ 30 Mpc, both are complete relative to the Schechter function

for galaxies more luminous than $x_{1/2}$ (GWGC contains galaxies only out to 100 Mpc, while GLADE extends farther). This is the original motivation for focusing on the top 50% of the luminosity (or mass) distributions: galaxy catalogs are complete for galaxies brighter than $x_{1/2}$ out to the relevant distances for GW NS–NS and NS–BH detections. In fact, we find that GLADE is complete out to ~ 300 Mpc for such galaxies (Fig. 3). In addition, NS–NS mergers are expected in galaxies with a B -band luminosity of roughly L_B^* , since most short GRBs have been seen to occur in such galaxies (Berger 2014).

We find some peculiar overabundances of galaxies in both versions of the GLADE catalog for $L_B/L_B^* \approx 1$ at 33–67 Mpc and in version 2 of the GLADE catalog near $x_{1/2}$ at < 17 Mpc. These overabundances lead to $> 100\%$ completeness values compared to the Schechter function at those distances in Figure 3, and may be due to artifacts in the GLADE catalog.

3.2. Galaxy Prioritization

For maximizing the efficiency of optical follow-up observations of GW triggers, we wish to prioritize galaxies that are in higher probability regions of the GW localization and which are more massive (assuming compact object mergers follow the mass distribution). Everything else being equal among those, we will prefer galaxies that are closer to us, in which a possible counterpart is more likely to be detected. This is a slightly different approach than the one outlined by Singer et al. (2016).

We include only galaxies that are inside the 99% GW localization region and less than 3σ away from the GW distance estimate (these criteria are relaxed to 99.995% and 5σ if the original cut leaves no galaxies). Second, we remove galaxies that are fainter than $x_{1/2}$ (or a lower threshold to make sure that at least 100 galaxies remain) based on a Schechter function with $\alpha = -1.07$ and an L^* corresponding to $M_B = -20.7$ (this is similar but not identical to the magnitude of -20.47 used by G16).

Of the galaxies that remain after the position, distance, and luminosity cuts, each is given three scores (which we detail below) based on

1. its location in the GW localization region (including distance information), S_{loc} ,
2. its absolute B -band luminosity (as an indicator of mass), S_{lum} , and
3. the likelihood of detecting a counterpart at its distance, S_{det} .

The localization information provided by the GW detectors includes a probability for each position of the sky, so that the probability of the true GW source to be

at a certain R.A. and decl. is a given $p_{\text{pos}}(\text{R.A.}, \text{decl.})$. The localization also includes a mean distance estimate μ_{dist} , standard deviation σ_{dist} , and normalization N_{dist} per R.A. and decl. We assume that the distance estimate probability function is a Gaussian with the provided mean, standard deviation, and normalization, so that the probability of the source being at distance D for a certain R.A. and decl. is:

$$p_{\text{dist}}(\text{R.A.}, \text{decl.}, D) = N_{\text{dist}}(\text{R.A.}, \text{decl.}) \cdot e^{-\frac{[D - \mu_{\text{dist}}(\text{R.A.}, \text{decl.})]^2}{2\sigma_{\text{dist}}^2(\text{R.A.}, \text{decl.})}}. \quad (1)$$

The location score of a galaxy at a certain RA, decl. and distance D is then

$$S_{\text{loc}} = p_{\text{pos}}(\text{R.A.}, \text{decl.}) \times p_{\text{dist}}(\text{R.A.}, \text{decl.}, D). \quad (2)$$

We then calculate the B -band luminosity of the galaxy, L_B (based on the B -band magnitude and distance provided in the GLADE catalog), and assign it a score

$$S_{\text{lum}} = \frac{L_B}{\sum L_B}, \quad (3)$$

where the sum is over all of the galaxies being considered.

Finally, we score each galaxy on the likelihood of detecting a counterpart there. We assume a limiting magnitude for our exposures, m_{lim} , and convert it to a limiting luminosity at the distance of each galaxy, L_{lim} . We also define the likely counterpart magnitude range, $M_{\text{KN}, \text{min}} - M_{\text{KN}, \text{max}}$ and convert those magnitudes to luminosities. We then give each galaxy a detection likelihood score,

$$S_{\text{det}} = \frac{L_{\text{KN}, \text{max}} - L_{\text{lim}}}{L_{\text{KN}, \text{max}} - L_{\text{KN}, \text{min}}} \quad (4)$$

while limiting it to being between 0.01 and 1. So, for example, a galaxy for which our limiting luminosity is equal to or fainter than the minimum luminosity we expect from the counterpart (i.e. we are guaranteed to see it) receives a detectability score of 1, while a galaxy for which our limiting magnitude is equal to or brighter than the maximum luminosity we expect from the counterpart (i.e. we will not see it) receives a detectability score of 0.01 (we avoid giving it a score of 0 in order to not exclude distant galaxies completely). We use a conservative selection of parameters ($m_{\text{lim}} = 22$, $M_{\text{KN}, \text{min}} = -17$ and $M_{\text{KN}, \text{max}} = -12$), making this score quite high for most galaxies in the NS-NS and NS-BH O2 detectability range of LIGO/Virgo. This criterion therefore has no effect on very close events, and will only slightly prefer closer galaxies in events around ~ 100 Mpc.

The product of these three scores is the final score assigned to each galaxy,

$$S = S_{\text{loc}} \times S_{\text{lum}} \times S_{\text{det}}. \quad (5)$$

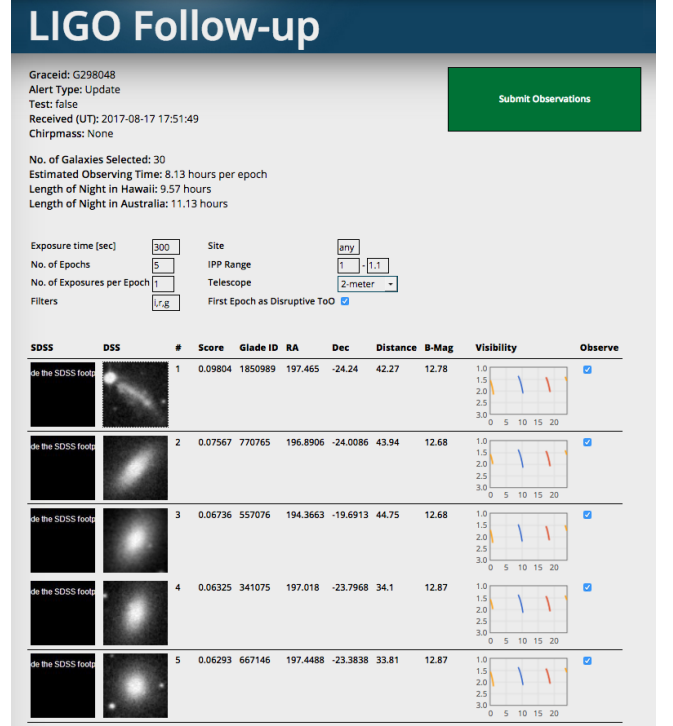


Figure 4. Screenshot of the web interface used for verifying the galaxies selected for monitoring following a GW trigger, ordered in descending priority (only the top 5 galaxies of 100 displayed are shown here). The galaxies to be observed and the observing parameters can be modified by the user before submitting the observations to the LCO scheduler. This screenshot shows the webpage generated following the G298048 trigger for GW170817. The galaxy containing the optical counterpart can be seen in the list (galaxy number 5). In principle, these fields can be sent to the LCO telescopes automatically within seconds of the alert being received, without any human intervention.

This score is then used to prioritize which galaxies to observe following a trigger. In Section 4.2 we show that this prioritization procedure ranked the correct host galaxy of a GW source as fifth out of the entire GLADE catalog.

3.3. The Triggering Process

We employ a GCN listener, based on `pyGCN`⁴, to receive LIGO/Virgo alerts via VOEvent (Seaman et al. 2011), ingest them to a database, download the Singer & Price (2016) HEALPIX localization map (which includes a distance constraint) attached to the alert, cross-check that localization with the GLADE galaxy catalog, and prioritize the galaxies to be observed according to the algorithm described above⁵. This process takes a few seconds, after which the top galaxies on the list can be sent to the LCO scheduler automatically. The observing requests use Intra-Proposal Priority (IPP) values pro-

⁴ <https://github.com/lpsinger/pygcn>

⁵ <https://github.com/svasily/pygcn>

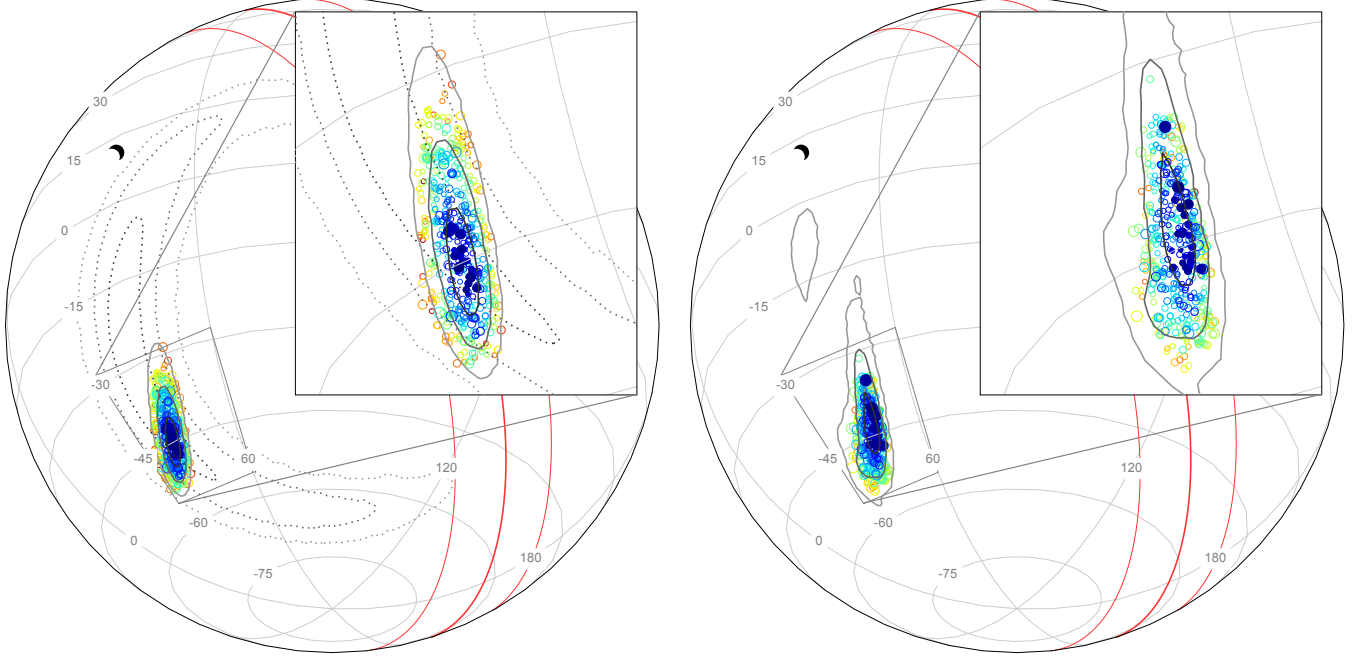


Figure 5. Localization region (contours) and the matched galaxies (circles) for G279595 (observed galaxies are in filled circles). The orthographic projection on the left is for the initial localization (LIGO only shown in dashed lines, LIGO/Virgo in solid lines), while the one on the right is for the updated localization. The contours indicate 50%, 90%, and 99% confidence bounds. The colors of the circles denote the priority of the galaxies (low priority in yellow, high priority in blue). The position of the plane of the Milky Way is indicated in red lines, with a $\pm 10^\circ$ -wide band. The position of the moon at the time of the trigger is indicated with a crescent symbol. Insets show a more detailed view of each localization.

portional to the priorities determined for the galaxies. IPP is used by the LCO scheduler to resolve scheduling conflicts if not all targets can be observed⁶.

During O2 we take the precaution of having humans verify the candidate galaxies to be observed before the triggers are delivered to the LCO scheduler. This verification step is done through a webpage (Fig. 4) which displays the top 100 galaxies selected sorted by priority, with the first 30 galaxies automatically selected. For each galaxy we present an SDSS cutout image, if available, a Digital Sky Survey (DSS) image, and the observability of the galaxy from the various LCO sites. The user can change the selection of galaxies and compare the total estimated observing time needed for each selection to the available length of night time at two representative LCO sites (Australia and Hawaii). The default exposure sequence is 300 seconds in each of the g, r and i filters to be taken with the 2-meter telescopes. This exposure time was chosen in order to reach a signal to noise of 10 at the expected magnitudes listed above for the different emission mechanisms for a kilonova at 100 Mpc. The number of galaxies selected by default (30) is the typical number that could fit in a full observing night given these exposure times, and is also the

amount predicted by G16 to contain roughly 50% of the mass in the localization region. However, the user can change the exposure times, numbers, filters, and telescope class based on the specific trigger parameters. The user can also select whether to submit the first epoch as a rapid response observation (which interrupts observations that were ongoing at the time of the trigger).

Once the galaxies, exposure sequences, number of epochs, and telescope class are selected, the information is converted into observing sequences which are then submitted programmatically to the LCO scheduler using its API. After the images are taken, they are automatically ingested and processed by the LCOGTSNpipe pipeline (Valenti et al. 2016) and displayed on a webpage for manual scanning, next to SDSS (if available) and DSS images of the field for comparison. Image subtraction can then be performed in order to detect faint transients using SDSS templates when available or subtracting the different LCO epochs off of each other to search for changing sources, otherwise.

4. ADVANCED LIGO/VIRGO OBSERVING RUN 2

O2 ran from 2016 November 30 to 2017 August 25, with Virgo joining the two LIGO detectors on 2017 August 01 (UT used throughout). Both LIGO detectors were taken offline on 2017 May 08 for commissioning activities, with the Livingston detector resuming opera-

⁶ https://lco.global/files/User_Documentation/the_new_priority_factor.pdf

tions on 2017 May 26 and the Hanford one on 2017 June 08. Several triggers were issued for follow-up to the EM community. Here we detail our follow-up observations for two such triggers.

4.1. *G297595 / GW170814*

G297595 was the first event detected by both LIGO detectors and the Virgo detector in real time, with the Virgo detection contributing significantly to the localization (LIGO Scientific Collaboration & Virgo Collaboration 2017a). The Virgo detection decreased the 50% (90%) localization region from 333 deg^2 (1158 deg^2) to 22 deg^2 (97 deg^2). The signal was identified on 2017 August 14 10:30:43 with a very low false-alarm rate (~ 1 per 80,000 years LIGO Scientific Collaboration & Virgo Collaboration 2017d), as a likely BH-BH merger at $\sim 500 \text{ Mpc}$. Despite the lack of a NS component and the large distance, we triggered our follow-up program given the relatively small localization region.

Following the VOEvent trigger sent at 2017 August 14 11:01:49, and the circular issued at 12:28:42 (LIGO Scientific Collaboration & Virgo Collaboration 2017d), we triggered 2-meter follow-up imaging of 30 galaxies

at 15:18:43 (Fig. 5, left panel). On 2017 August 16 07:02:19 an updated localization was issued. The region moved east and grew slightly to 36 deg^2 (190 deg^2) for the 50% (90%) localization probability, due to marginalization over calibration uncertainties (LIGO Scientific Collaboration & Virgo Collaboration 2017e). The updated localization was sent by VOEvent at 17:01:54. We stopped all of our ongoing observation requests at 21:37:35 and re-submitted a new set of 30 galaxies based on the updated localization at 21:39:24 (Fig. 5, right panel). In total, 63 images were obtained for 20 galaxies, 16 from the original localization (Table 3; the initial measurements of which were reported in Hosseinzadeh et al. 2017) and four from the updated localization (Table 4). Upper limits are calculated by calibrating a local sequence of stars in each field to the AAVSO Photometric All-Sky Survey (APASS) catalog (Henden et al. 2009) and are presented in the AB system with no extinction corrections applied.

No obvious optical counterparts were detected. All observations from this trigger were stopped on 2017 August 17 23:04:02 in order to free the telescopes to aggressively pursue the next trigger.

Table 3. LCO follow-up observations of the initial LIGO/Virgo localization for trigger G297595 in descending order of galaxy priority. The leftmost four columns are provided as-is from the GLADE catalog. A limiting magnitude was not calculated for fields with very few APASS stars visible. All exposures were 300 seconds long. See Table 1 for the list of site abbreviations used in the telescope column.

GLADE ID	RA	Dec	Distance [Mpc]	m_B	L_B/L_B^*	UT	Telescope	Filt.	Limiting Mag. (3σ)
723415	40.523499	-45.337452	432	15.57	5.808	2017-08-14 16:46:38	COJ 2m	g	21.52
723415	40.523499	-45.337452	432	15.57	5.808	2017-08-14 16:52:10	COJ 2m	r	21.17
723415	40.523499	-45.337452	432	15.57	5.808	2017-08-14 16:57:41	COJ 2m	i	20.41
721389	42.015915	-44.111561	476	16.09	4.365	2017-08-14 16:00:52	COJ 2m	g	21.35
721389	42.015915	-44.111561	476	16.09	4.365	2017-08-14 16:08:39	COJ 2m	r	21.41
721389	42.015915	-44.111561	476	16.09	4.365	2017-08-14 16:14:12	COJ 2m	i	21.66
787654	40.73167	-44.360573	442	16.18	3.467	2017-08-14 17:06:51	COJ 2m	g	20.77
787654	40.73167	-44.360573	442	16.18	3.467	2017-08-14 17:12:22	COJ 2m	r	18.89
787654	40.73167	-44.360573	442	16.18	3.467	2017-08-14 17:17:53	COJ 2m	i	21.56
556821	41.190659	-45.095711	440	16.63	2.270	2017-08-14 18:20:21	COJ 2m	g	20.26
556821	41.190659	-45.095711	440	16.63	2.270	2017-08-14 18:26:34	COJ 2m	r	18.99
556821	41.190659	-45.095711	440	16.63	2.270	2017-08-14 18:32:06	COJ 2m	i	17.48
625999	41.654194	-42.367088	307	14.42	8.472	2017-08-15 14:28:10	OGG 2m	g	21.82
625999	41.654194	-42.367088	307	14.42	8.472	2017-08-15 14:34:20	OGG 2m	r	22.01
625999	41.654194	-42.367088	307	14.42	8.472	2017-08-15 14:39:52	OGG 2m	i	21.82
625999	41.654194	-42.367088	307	14.42	8.472	2017-08-15 15:08:26	OGG 2m	g	21.36
706152	40.122471	-45.386868	494	16.78	2.489	2017-08-15 13:30:24	COJ 2m	g	20.38
706152	40.122471	-45.386868	494	16.78	2.489	2017-08-15 13:35:57	COJ 2m	r	20.53

Table 3 continued

Table 3 (*continued*)

GLADE ID	RA	Dec	Distance [Mpc]	m_B	L_B/L_B^*	UT	Telescope	Filt.	Limiting Mag. (3σ)
706152	40.122471	-45.386868	494	16.78	2.489	2017-08-15 13:41:28	COJ 2m	i	20.22
752527	42.434814	-42.327412	322	15.05	5.200	2017-08-15 14:47:23	OGG 2m	g	0.00
752527	42.434814	-42.327412	322	15.05	5.200	2017-08-15 14:52:54	OGG 2m	r	0.00
752527	42.434814	-42.327412	322	15.05	5.200	2017-08-15 14:58:25	OGG 2m	i	0.00
1066576	41.292435	-46.59705	398	16.49	2.113	2017-08-14 17:27:53	COJ 2m	g	21.37
1066576	41.292435	-46.59705	398	16.49	2.113	2017-08-14 17:33:24	COJ 2m	r	21.50
1066576	41.292435	-46.59705	398	16.49	2.113	2017-08-14 17:38:56	COJ 2m	i	21.52
1005823	42.07933	-44.054893	450	16.89	1.863	2017-08-15 14:10:58	COJ 2m	g	20.53
1005823	42.07933	-44.054893	450	16.89	1.863	2017-08-15 14:16:30	COJ 2m	r	20.65
1005823	42.07933	-44.054893	450	16.89	1.863	2017-08-15 14:22:02	COJ 2m	i	20.34
1031304	41.217548	-46.500435	401	16.63	1.893	2017-08-15 14:53:00	COJ 2m	g	20.87
1031304	41.217548	-46.500435	401	16.63	1.893	2017-08-15 14:58:31	COJ 2m	r	20.84
1031304	41.217548	-46.500435	401	16.63	1.893	2017-08-15 15:04:03	COJ 2m	i	20.63
622864	41.392635	-44.539589	316	15.47	3.404	2017-08-14 19:12:39	COJ 2m	g	20.45
622864	41.392635	-44.539589	316	15.47	3.404	2017-08-14 19:18:10	COJ 2m	r	20.17
622864	41.392635	-44.539589	316	15.47	3.404	2017-08-14 19:23:41	COJ 2m	i	19.91
1415752	42.418404	-44.226032	421	16.77	1.832	2017-08-15 13:49:58	COJ 2m	g	20.43
1415752	42.418404	-44.226032	421	16.77	1.832	2017-08-15 13:55:31	COJ 2m	r	20.59
1415752	42.418404	-44.226032	421	16.77	1.832	2017-08-15 14:01:02	COJ 2m	i	20.27
1181112	41.086727	-43.939903	452	16.86	1.930	2017-08-15 14:32:00	COJ 2m	g	20.76
1181112	41.086727	-43.939903	452	16.86	1.930	2017-08-15 14:37:31	COJ 2m	r	20.75
1181112	41.086727	-43.939903	452	16.86	1.930	2017-08-15 14:43:03	COJ 2m	i	20.59
806902	42.062664	-45.159618	446	16.93	1.770	2017-08-14 16:25:24	COJ 2m	g	20.79
806902	42.062664	-45.159618	446	16.93	1.770	2017-08-14 16:30:55	COJ 2m	r	18.41
806902	42.062664	-45.159618	446	16.93	1.770	2017-08-14 16:36:27	COJ 2m	i	20.71
1647694	42.0008	-46.31986	381	16.24	2.443	2017-08-14 18:52:50	COJ 2m	g	21.47
1647694	42.0008	-46.31986	381	16.24	2.443	2017-08-14 18:59:02	COJ 2m	r	21.52
1647694	42.0008	-46.31986	381	16.24	2.443	2017-08-14 19:04:33	COJ 2m	i	20.50
62667	41.574863	-44.984894	487	17.22	1.619	2017-08-15 15:14:03	COJ 2m	g	20.78
62667	41.574863	-44.984894	487	17.22	1.619	2017-08-15 15:19:34	COJ 2m	r	20.88
62667	41.574863	-44.984894	487	17.22	1.619	2017-08-15 15:25:06	COJ 2m	i	20.54

Table 4. LCO follow-up observations of the updated LIGO/Virgo localization for trigger G297595 in descending order of galaxy priority. The leftmost four columns are provided as-is from the GLADE catalog. All exposures were 300 seconds long. See Table 1 for the list of site abbreviations used in the telescope column.

GLADE ID	RA	Dec	Distance [Mpc]	m_B	L_B/L_B^*	UT	Telescope	Filt.	Limiting Mag. (3σ)
789138	49.259586	-40.445934	414	14.86	10.280	2017-08-17 17:37:02	COJ 2m	g	21.75

Table 4 *continued*

Table 4 (*continued*)

GLADE ID	RA	Dec	Distance [Mpc]	m_B	L_B/L_B^*	UT	Telescope	Filt.	Limiting Mag. (3σ)
789138	49.259586	−40.445934	414	14.86	10.280	2017-08-17 17:44:49	COJ 2m	r	21.86
789138	49.259586	−40.445934	414	14.86	10.280	2017-08-17 17:50:20	COJ 2m	i	21.60
632134	49.61784	−42.020428	420	15.30	7.047	2017-08-17 16:18:03	COJ 2m	g	21.95
632134	49.61784	−42.020428	420	15.30	7.047	2017-08-17 16:23:33	COJ 2m	r	21.94
632134	49.61784	−42.020428	420	15.30	7.047	2017-08-17 16:29:04	COJ 2m	i	21.59
1385568	45.634289	−46.345387	455	16.66	2.353	2017-08-17 13:41:49	COJ 2m	g	21.22
1385568	45.634289	−46.345387	455	16.66	2.353	2017-08-17 13:47:22	COJ 2m	r	21.47
1385568	45.634289	−46.345387	455	16.66	2.353	2017-08-17 17:57:11	COJ 2m	g	21.87
1385568	45.634289	−46.345387	455	16.66	2.353	2017-08-17 18:02:42	COJ 2m	r	22.19
1385568	45.634289	−46.345387	455	16.66	2.353	2017-08-17 18:08:14	COJ 2m	i	21.77
712985	48.530678	−42.086346	440	16.17	3.467	2017-08-17 14:43:49	OGG 2m	g	21.62
712985	48.530678	−42.086346	440	16.17	3.467	2017-08-17 14:49:22	OGG 2m	r	22.41
712985	48.530678	−42.086346	440	16.17	3.467	2017-08-17 14:54:52	OGG 2m	i	21.98

4.2. G298048 / GW170817

This event ([LIGO Scientific Collaboration & Virgo Collaboration 2017b,c](#)) was detected as a weak γ -ray transient, interpreted as a likely short GRB, by the Fermi Gamma-ray Burst Monitor (GBM) on 2017 August 17 12:41:06 ([Connaughton et al. 2017](#)) and then associated with a low false-alarm rate (~ 1 in 10,000 years), likely NS–NS merger GW event detected two seconds earlier in the LIGO Hanford detector ([LIGO Scientific Collaboration & Virgo Collaboration 2017f](#)). The GBM localization was distributed at 13:47:37 via GCN Circular before a full LIGO/Virgo localization was available. The initial GW localization (solely from the Hanford detector, thus covering most of the sky, with a preliminary distance estimate) was distributed via VO-Event at 13:08:16. We triggered a first set of 11 galaxies selected from the GW localization, chosen to lie near the GBM localization center for LCO 1-m imaging starting at 16:34:34 (Fig. 6, left panel). We obtained a total of 30 images of eight galaxies (Table 5), which we immediately inspected for transients and found none.

A LIGO/Virgo localization, consistent with the GBM region but offset from its center, was distributed by VOEvent at 17:51:48. A total of 182 galaxies were identified by our algorithm in the LIGO/Virgo localization region (adhering to the criteria detailed in Section 3.2). We triggered LCO 0.4-m and 1-m imaging of the top 60 galaxies in the prioritized galaxy list starting at 22:36:19 (Fig. 6, right panel), and stopped observations of the previous GBM-selected galaxies shortly thereafter. Given the limited observability of the up-

dated GW localization region to the first 1.5–2 hours of the night, we decided to trigger single 300-second w -band exposures in order to be able to cover many galaxies in this short window. We obtained a total of 96 images of the triggered 60 galaxies (Table 6), which constitute 85% of the luminosity contained in the 182 identified galaxies (Fig. 7).

The optical counterpart, AT 2017gfo, announced by [Coulter et al. \(2017\)](#) was in one of our observed galaxies, ranked fifth in priority. The transient is clearly present in our imaging of that galaxy, beginning with our first epoch ([Arcavi et al. 2017b](#)) taken approximately one hour before the [Coulter et al. \(2017\)](#) announcement. We continued to monitor other galaxies in case AT 2017gfo turned out to be an unrelated transient, but as it became clear that the color and luminosity of AT 2017gfo were evolving rapidly, we gradually shifted towards observing just that position with more bands and more telescopes. No obvious counterpart candidates were found in the other galaxies surveyed. The follow-up data obtained for AT 2017gfo is the topic of two companion papers ([Arcavi et al. 2017a](#); [McCully et al. 2017](#)).

5. SUMMARY

We have presented an implementation of the [G16](#) galaxy-targeted GW follow-up strategy using the GLADE catalog and the LCO network of telescopes. We show that the GLADE catalog is complete for galaxies brighter than $x_{1/2}$ (the median luminosity of galaxies according to a Schechter function) out to 300 Mpc. We detail our algorithm for selecting and prioritizing

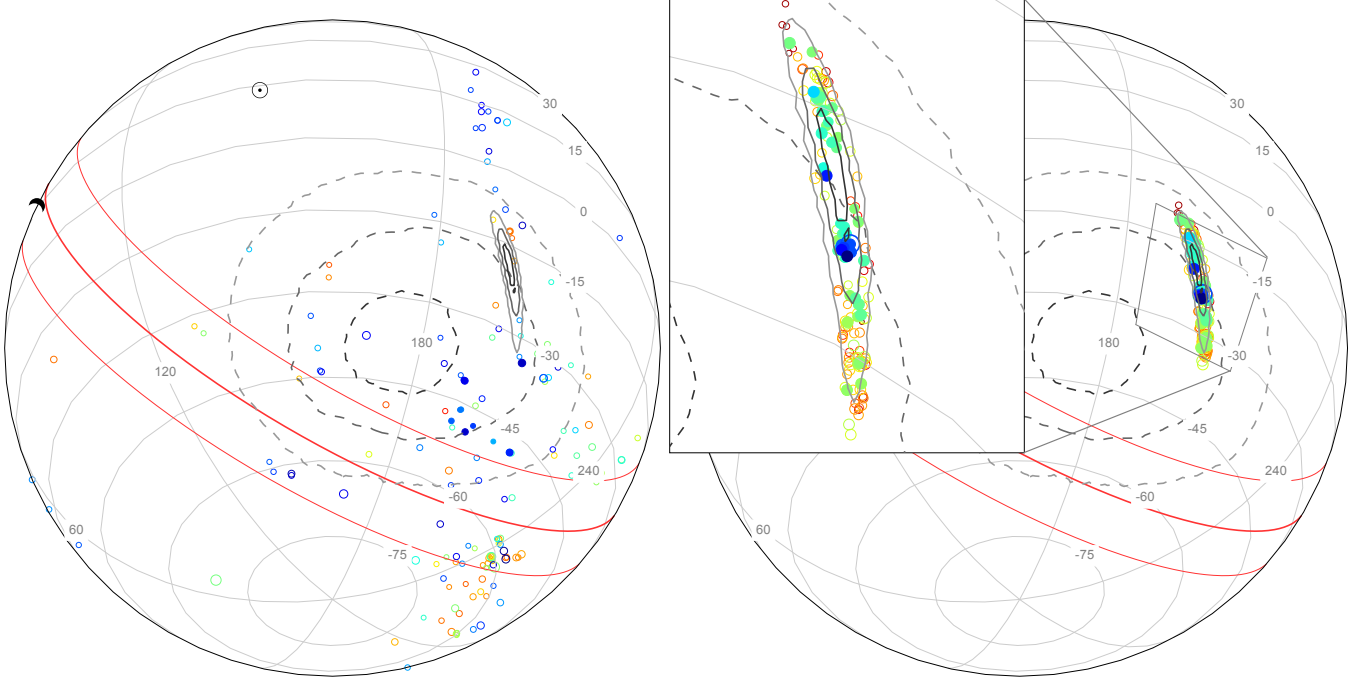


Figure 6. Localization region (contours) and the matched galaxies (circles) for G298048. The orthographic projection on the left shows the galaxies selected for observations (filled circles) following the initial LIGO localization (which covered most of the sky; not shown) and Fermi localization (dashed contours), while the one on the right is for the updated LIGO/Virgo localization (solid contours). The contours indicate 50%, 90%, and 99% confidence bounds. The colors of the circles denote the priority of the galaxies (low priority in yellow, high priority in blue). The position of the plane of the Milky Way is indicated in red lines, with a $\pm 10^\circ$ -wide band. The position of the moon is indicated with the a crescent symbol, and that of the sun with a \odot symbol. The inset shows a more detailed view of the LIGO/Virgo localization. The galaxy containing the optical counterpart is marked with an additional circle around it.

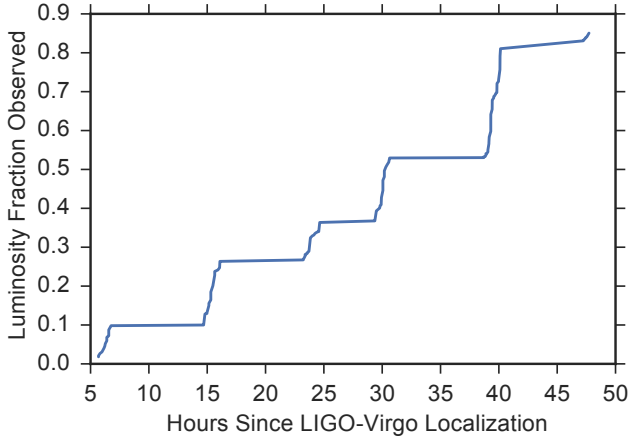


Figure 7. Cumulative luminosity observed as a fraction of the total luminosity contained in the 182 galaxies identified by our algorithm in the LIGO/Virgo localization region of GW170817. Due to the short visibility window of the localization region (only ~ 2 hours per night), it took approximately 30 hours to cover half of the luminosity. Given the importance of the trigger as the first NS-NS detection, we continued to observe additional galaxies until we reached 85% of the total galaxy luminosity.

these galaxies using a GW localization and distance constraint, and taking into account the observing capabil-

ities of LCO and the expected luminosity range of optical counterparts to NS-NS and NS-BH mergers. We discuss the results of using this strategy following two different triggers. For the second trigger, our algorithm selected the correct host galaxy as fifth in priority from the list of 182 galaxies identified in the LIGO/Virgo localization region. This allowed us to obtain early data of the counterpart (Arcavi et al. 2017a).

The galaxy prioritization algorithm presented here can be adapted to any telescope with very minor adjustments. Given the large distance to which the GLADE catalog is complete for galaxies brighter than the median galaxy luminosity, our follow-up strategy will remain relevant for following NS-NS and NS-BH GW triggers in O3.

We thank J. Canizzo for information on the G16 completeness plots, V. Connaughton and A. Goldstein for providing us with the Fermi GBM HEALPIX map for GRB170817A, S. Guruswamy for mentorship during S. Vasylyev’s summer internship at LCO, and the LVC-EM liaisons for their guidance and assistance. Support for I.A. and J.B. was provided by NASA through the Einstein Fellowship Program, grants PF6-170148 and

PF7-180162, respectively. C.M., G.H. and D.A.H. are supported by NSF grant AST-1313484. S. Vasylyev was supported by a SURF fellowship from the UCSB College of Creative Studies. D.P. and D.M. acknowledge support by ISF grant 541/17. T.P. is supported by an ERC advanced grant. D.K. is supported in part by a Department of Energy (DOE) Early Career award DE-

SC0008067, a DOE Office of Nuclear Physics award DE-SC0017616, and a DOE SciDAC award DE-SC0018297, and by the Director, Office of Energy Research, Office of High Energy and Nuclear Physics, Divisions of Nuclear Physics, of the U.S. Department of Energy under Contract No.DE-AC02-05CH11231. This work made use of the LCO network.

Table 5. LCO follow-up observations of the Fermi GBM trigger of GRB170817A in descending order of galaxy priority. The leftmost four columns are provided as-is from the GLADE catalog. All exposures were 300 seconds long. See Table 1 for the list of site abbreviations used in the telescope column.

GLADE ID	RA	Dec	Distance [Mpc]	m_B	L_B/L_B^*	UT	Telescope	Filt.	Limiting Mag. (3σ)
732352	204.16272	-33.965916	49	11.24	4.042	2017-08-17 18:05:34	CPT 1m	g	21.88
732352	204.16272	-33.965916	49	11.24	4.042	2017-08-17 18:11:31	CPT 1m	r	21.70
732352	204.16272	-33.965916	49	11.24	4.042	2017-08-17 18:17:29	CPT 1m	i	21.10
1306036	198.491943	-49.478775	45	11.47	2.778	2017-08-17 18:05:34	CPT 1m	g	22.78
1306036	198.491943	-49.478775	45	11.47	2.778	2017-08-17 18:11:30	CPT 1m	r	22.30
1306036	198.491943	-49.478775	45	11.47	2.778	2017-08-17 18:17:27	CPT 1m	i	22.02
564852	214.019012	-48.127373	54	11.69	3.280	2017-08-17 18:23:50	CPT 1m	g	21.66
564852	214.019012	-48.127373	54	11.69	3.280	2017-08-17 18:29:46	CPT 1m	r	21.69
564852	214.019012	-48.127373	54	11.69	3.280	2017-08-17 23:13:25	LSC 1m	g	21.70
564852	214.019012	-48.127373	54	11.69	3.280	2017-08-17 23:19:21	LSC 1m	r	21.77
564852	214.019012	-48.127373	54	11.69	3.280	2017-08-17 23:25:16	LSC 1m	i	21.56
2037	199.749649	-47.908653	40	11.80	1.675	2017-08-17 17:47:54	CPT 1m	g	22.03
2037	199.749649	-47.908653	40	11.80	1.675	2017-08-17 17:53:51	CPT 1m	r	21.79
2037	199.749649	-47.908653	40	11.80	1.675	2017-08-17 18:23:37	CPT 1m	g	21.66
2037	199.749649	-47.908653	40	11.80	1.675	2017-08-17 18:29:33	CPT 1m	r	21.50
2037	199.749649	-47.908653	40	11.80	1.675	2017-08-17 23:13:26	LSC 1m	g	21.32
2037	199.749649	-47.908653	40	11.80	1.675	2017-08-17 23:19:22	LSC 1m	r	23.09
2037	199.749649	-47.908653	40	11.80	1.675	2017-08-17 23:25:19	LSC 1m	i	22.87
815140	193.363815	-48.749153	49	11.98	2.081	2017-08-17 17:24:22	CPT 1m	g	21.38
815140	193.363815	-48.749153	49	11.98	2.081	2017-08-17 17:30:18	CPT 1m	r	21.64
815140	193.363815	-48.749153	49	11.98	2.081	2017-08-17 17:36:15	CPT 1m	i	20.97
1850978	194.305	-46.37728	46	12.12	1.644	2017-08-17 17:24:20	CPT 1m	g	21.90
1850978	194.305	-46.37728	46	12.12	1.644	2017-08-17 17:30:17	CPT 1m	r	21.60
1850978	194.305	-46.37728	46	12.12	1.644	2017-08-17 17:36:14	CPT 1m	i	21.12
621160	194.532623	-46.264214	29	10.93	1.923	2017-08-17 17:05:17	CPT 1m	g	21.38
621160	194.532623	-46.264214	29	10.93	1.923	2017-08-17 17:11:14	CPT 1m	r	21.50
621160	194.532623	-46.264214	29	10.93	1.923	2017-08-17 17:17:10	CPT 1m	i	21.14
737707	213.977814	-48.114883	59	12.06	2.826	2017-08-17 17:05:48	CPT 1m	g	21.23
737707	213.977814	-48.114883	59	12.06	2.826	2017-08-17 17:11:47	CPT 1m	r	21.53
737707	213.977814	-48.114883	59	12.06	2.826	2017-08-17 17:17:43	CPT 1m	i	21.47

Table 6. LCO follow-up observations of LIGO/Virgo localization for GW170817 in descending order of galaxy priority. The leftmost four columns are provided as-is from the GLADE catalog. The galaxy which hosted the optical counterpart has GLADE ID 667146, and is fifth on this prioritized list. All exposures were 300 seconds long. See Table 1 for the list of site abbreviations used in the telescope column.

GLADE ID	RA	Dec	Distance [Mpc]	m_B	L_B/L_B^*	UT	Telescope	Filt.	Limiting Mag. (3σ)
1850989	197.465	-24.24	42	12.78	0.724	2017-08-18 00:25:23	LSC 1m	w	21.89
1850989	197.465	-24.24	42	12.78	0.724	2017-08-19 00:02:51	LSC 1m	w	21.81
770765	196.89064	-24.008606	43	12.68	0.859	2017-08-17 23:32:42	LSC 1m	w	23.07
770765	196.89064	-24.008606	43	12.68	0.859	2017-08-18 23:55:24	LSC 1m	w	23.19
557076	194.366257	-19.691298	44	12.68	0.890	2017-08-18 09:00:23	COJ 1m	w	20.98
557076	194.366257	-19.691298	44	12.68	0.890	2017-08-18 23:47:56	LSC 1m	w	21.71
341075	197.018005	-23.796844	34	12.87	0.434	2017-08-18 00:00:22	LSC 1m	w	21.68
341075	197.018005	-23.796844	34	12.87	0.434	2017-08-19 00:02:48	LSC 1m	w	22.79
667146	197.448776	-23.383831	33	12.87	0.427	2017-08-18 00:15:23	LSC 1m	w	21.52
667146	197.448776	-23.383831	33	12.87	0.427	2017-08-18 09:10:23	COJ 1m	w	21.55
1366038	197.691406	-23.865728	33	12.64	0.515	2017-08-18 00:37:24	LSC 1m	w	21.70
1366038	197.691406	-23.865728	33	12.64	0.515	2017-08-19 00:30:02	LSC 1m	w	21.86
1478047	197.466	-24.23937	38	13.60	0.283	2017-08-17 23:40:22	LSC 1m	w	21.88
1478047	197.466	-24.23937	38	13.60	0.283	2017-08-19 00:25:22	LSC 1m	w	21.76
602087	196.774902	-23.67704	33	13.18	0.313	2017-08-18 00:07:49	LSC 1m	w	21.90
602087	196.774902	-23.67704	33	13.18	0.313	2017-08-19 00:17:50	LSC 1m	w	21.83
773496	196.735474	-23.91707	33	13.07	0.352	2017-08-18 00:15:23	LSC 1m	w	22.87
773496	196.735474	-23.91707	33	13.07	0.352	2017-08-18 23:38:53	LSC 1m	w	23.13
645472	196.907242	-23.57892	41	14.21	0.189	2017-08-17 23:50:35	LSC 1m	w	21.87
645472	196.907242	-23.57892	41	14.21	0.189	2017-08-18 23:13:50	LSC 1m	w	20.58
3644	192.248566	-14.399235	49	12.55	1.232	2017-08-18 08:39:33	COJ 1m	w	21.08
3644	192.248566	-14.399235	49	12.55	1.232	2017-08-18 23:55:24	LSC 1m	w	21.71
626	193.998657	-19.26899	41	13.27	0.454	2017-08-18 09:30:25	COJ 1m	w	21.84
626	193.998657	-19.26899	41	13.27	0.454	2017-08-19 00:10:24	LSC 1m	w	21.55
1486718	196.937	-22.85784	26	12.88	0.265	2017-08-18 00:05:02	LSC 1m	w	21.94
1486718	196.937	-22.85784	26	12.88	0.265	2017-08-18 23:40:41	LSC 1m	w	21.76
684330	193.363464	-17.005495	54	12.76	1.223	2017-08-18 09:30:25	COJ 1m	w	21.48
684330	193.363464	-17.005495	54	12.76	1.223	2017-08-18 23:21:45	LSC 1m	w	21.07
777014	196.270554	-22.383947	30	13.98	0.125	2017-08-17 23:32:43	LSC 1m	w	22.06
777014	196.270554	-22.383947	30	13.98	0.125	2017-08-18 23:46:19	LSC 1m	w	22.36
708169	196.666443	-22.455793	42	15.15	0.081	2017-08-18 08:33:18	COJ 1m	w	19.32
708169	196.666443	-22.455793	42	15.15	0.081	2017-08-19 17:15:24	CPT 1m	w	22.13
1486724	197.329	-24.38456	33	13.85	0.169	2017-08-18 00:25:23	LSC 1m	w	21.82
1486724	197.329	-24.38456	33	13.85	0.169	2017-08-19 17:25:22	CPT 1m	w	22.24
1486713	196.719	-22.84175	33	14.67	0.082	2017-08-18 08:50:25	COJ 1m	w	21.02
1486614	193.706	-16.0522	46	14.95	0.118	2017-08-18 08:40:32	COJ 1m	w	21.17
977319	194.252274	-17.320408	54	13.97	0.402	2017-08-19 17:35:24	CPT 1m	w	21.52
1486596	193.107	-15.51722	50	14.25	0.266	2017-08-18 09:00:26	COJ 1m	w	20.78
1490961	197.177	-23.77574	39	15.22	0.066	2017-08-18 18:20:21	CPT 1m	w	21.21

Table 6 continued

Table 6 (*continued*)

GLADE ID	RA	Dec	Distance [Mpc]	m_B	L_B/L_B^*	UT	Telescope	Filt.	Limiting Mag. (3σ)
1490961	197.177	-23.77574	39	15.22	0.066	2017-08-19 17:06:27	CPT 1m	w	21.68
420937	198.880432	-23.982388	35	12.32	0.776	2017-08-18 09:57:07	COJ 1m	w	21.64
635635	196.600052	-24.164007	33	13.78	0.180	2017-08-18 09:46:43	COJ 1m	w	21.68
635635	196.600052	-24.164007	33	13.78	0.180	2017-08-19 17:15:22	CPT 1m	w	21.67
7	192.519547	-14.73349	53	13.21	0.782	2017-08-18 09:21:21	COJ 1m	w	21.59
7	192.519547	-14.73349	53	13.21	0.782	2017-08-19 17:35:25	CPT 1m	w	21.90
795473	199.096786	-26.561554	44	13.95	0.271	2017-08-18 09:55:25	COJ 1m	w	22.04
645300	196.580811	-22.98033	39	15.71	0.042	2017-08-18 09:21:22	COJ 1m	w	21.63
645300	196.580811	-22.98033	39	15.71	0.042	2017-08-19 17:25:23	CPT 1m	w	21.75
1486721	197.135	-23.34725	44	15.71	0.054	2017-08-18 08:50:23	COJ 1m	w	20.93
646603	193.219254	-15.413292	56	13.09	0.961	2017-08-18 09:10:23	COJ 1m	w	21.50
646603	193.219254	-15.413292	56	13.09	0.961	2017-08-19 17:06:22	CPT 1m	w	21.24
1566	192.827362	-14.573568	51	13.80	0.427	2017-08-18 17:15:25	CPT 1m	w	21.25
3385	199.958435	-27.410082	27	10.97	1.644	2017-08-18 17:42:31	CPT 1m	w	23.25
3385	199.958435	-27.410082	27	10.97	1.644	2017-08-19 09:57:51	COJ 1m	w	22.84
1308288	196.907013	-23.938364	45	15.59	0.064	2017-08-18 18:15:26	CPT 1m	w	21.95
1308288	196.907013	-23.938364	45	15.59	0.064	2017-08-19 09:35:25	COJ 1m	w	22.57
3250	199.521057	-26.837221	24	11.10	1.117	2017-08-18 18:30:25	CPT 1m	w	21.30
3250	199.521057	-26.837221	24	11.10	1.117	2017-08-19 09:17:51	COJ 1m	w	21.56
2704	193.830368	-14.949816	43	14.31	0.185	2017-08-18 17:15:25	CPT 1m	w	21.76
2704	193.830368	-14.949816	43	14.31	0.185	2017-08-19 08:45:22	COJ 1m	w	21.19
1866	194.690292	-17.542887	54	14.87	0.175	2017-08-18 18:05:41	CPT 1m	w	21.81
1866	194.690292	-17.542887	54	14.87	0.175	2017-08-19 09:25:34	COJ 1m	w	21.38
4242	189.997894	-11.62307	9	8.52	1.959	2017-08-19 09:10:20	COJ 0.4m	w	19.75
1486716	196.782	-24.11136	27	14.07	0.090	2017-08-18 18:10:25	CPT 1m	w	21.58
1486716	196.782	-24.11136	27	14.07	0.090	2017-08-19 09:41:24	COJ 1m	w	21.86
665505	193.212875	-15.491673	50	15.38	0.095	2017-08-18 17:25:23	CPT 1m	w	21.95
665505	193.212875	-15.491673	50	15.38	0.095	2017-08-19 09:30:04	COJ 1m	w	21.75
1220861	192.654388	-14.482746	49	15.26	0.100	2017-08-18 17:25:21	CPT 1m	w	21.52
1220861	192.654388	-14.482746	49	15.26	0.100	2017-08-19 08:33:51	COJ 1m	w	20.17
761543	197.599045	-21.684093	35	13.85	0.190	2017-08-18 17:35:04	CPT 1m	w	22.19
761543	197.599045	-21.684093	35	13.85	0.190	2017-08-19 09:50:23	COJ 1m	w	21.74
720029	193.620285	-16.350813	55	14.90	0.179	2017-08-18 17:05:47	CPT 1m	w	20.65
720029	193.620285	-16.350813	55	14.90	0.179	2017-08-19 09:00:38	COJ 1m	w	21.83
1071538	192.717911	-14.906625	50	15.28	0.106	2017-08-18 18:00:19	CPT 1m	w	21.39
1071538	192.717911	-14.906625	50	15.28	0.106	2017-08-19 09:10:25	COJ 1m	w	21.36
2151	191.728119	-11.637039	29	13.26	0.233	2017-08-18 17:52:16	CPT 1m	w	21.49
2151	191.728119	-11.637039	29	13.26	0.233	2017-08-19 08:55:23	COJ 1m	w	21.05
1486720	197.064	-21.00158	34	15.19	0.053	2017-08-18 17:06:09	CPT 1m	w	21.19
1486720	197.064	-21.00158	34	15.19	0.053	2017-08-19 09:42:50	COJ 1m	w	21.38
1481025	197.324	-24.38207	38	16.50	0.019	2017-08-18 18:25:24	CPT 1m	w	21.85
1481025	197.324	-24.38207	38	16.50	0.019	2017-08-19 09:02:53	COJ 1m	w	21.59

Table 6 continued

Table 6 (*continued*)

GLADE ID	RA	Dec	Distance [Mpc]	m_B	L_B/L_B^*	UT	Telescope	Filt.	Limiting Mag. (3σ)
1486644	194.643	-16.80437	52	14.81	0.175	2017-08-19 08:55:20	COJ 0.4m	w	19.99
811204	201.209473	-30.307772	53	12.70	1.240	2017-08-19 09:57:15	COJ 0.4m	w	20.46
1490974	196.879	-23.17047	40	17.26	0.011	2017-08-19 08:40:19	COJ 0.4m	w	19.75
1490971	196.348	-23.52258	39	16.10	0.030	2017-08-19 08:50:11	COJ 0.4m	w	19.99
722418	198.573929	-26.58268	53	14.63	0.213	2017-08-19 09:35:20	COJ 0.4m	w	20.44
519820	201.013931	-32.341335	35	12.45	0.683	2017-08-19 09:02:15	COJ 0.4m	w	20.67
336095	201.988586	-31.499374	35	12.13	0.908	2017-08-19 10:00:14	COJ 0.4m	w	19.86
607497	199.752182	-27.628489	29	13.20	0.233	2017-08-19 09:50:10	COJ 0.4m	w	20.68
640513	192.717209	-14.491902	57	13.58	0.644	2017-08-19 09:10:11	COJ 0.4m	w	19.79
1486585	192.723	-14.33199	57	13.41	0.756	2017-08-19 09:00:29	COJ 0.4m	w	19.95
1486633	194.261	-19.51809	56	14.48	0.273	2017-08-19 09:25:20	COJ 0.4m	w	19.72
751761	197.648849	-21.748224	28	13.33	0.198	2017-08-19 08:45:22	COJ 0.4m	w	20.00
1478083	201.121	-30.43168	52	13.45	0.614	2017-08-19 09:17:16	COJ 0.4m	w	21.75
592826	199.083679	-28.285717	59	13.07	1.094	2017-08-19 09:42:13	COJ 0.4m	w	20.50
341078	194.386322	-19.700184	50	16.18	0.045	2017-08-19 08:33:32	COJ 0.4m	w	20.57

REFERENCES

- Abbott, B. P., Abbott, R., Abbott, T. D., et al. 2016a, *Physical Review X*, 6, 041015
- . 2016b, *Living Reviews in Relativity*, 19, 1
- Acernese, F., Agathos, M., Agatsuma, K., et al. 2015, *Classical and Quantum Gravity*, 32, 024001
- Arcavi, I., Hosseinzadeh, G., Howell, D. A., et al. 2017a, *Nature*, in press
- Arcavi, I., Howell, D. A., McCully, C., et al. 2017b, *GCN Circ.*, 21538
- Barnes, J., & Kasen, D. 2013, *ApJ*, 775, 18
- Berger, E. 2014, *ARA&A*, 52, 43
- Berger, E., Fong, W., & Chornock, R. 2013, *ApJL*, 774, L23
- Bilicki, M., Jarrett, T. H., Peacock, J. A., Cluver, M. E., & Steward, L. 2014, *ApJS*, 210, 9
- Brown, T. M., Baliber, N., Bianco, F. B., et al. 2013, *PASP*, 125, 1031
- Connaughton, V., Blackburn, L., Briggs, M. S., et al. 2017, *GCN Circ.*, 21506
- Coulter, D. A., Kilpatrick, C. D., Siebert, M. R., et al. 2017, *GCN Circ.*, 21529
- Dalya, G., Frei, Z., Galgoczi, G., Raffai, P., & de Souza, R. S. 2016, *VizieR Online Data Catalog*, 7275
- Eichler, D., Livio, M., Piran, T., & Schramm, D. N. 1989, *Nature*, 340, 126
- Fong, W., & Berger, E. 2013, *ApJ*, 776, 18
- Gehrels, N., Cannizzo, J. K., Kanner, J., et al. 2016, *ApJ*, 820, 136
- Goriely, S., Bauswein, A., & Janka, H.-T. 2011, *ApJL*, 738, L32
- Grossman, D., Korobkin, O., Rosswog, S., & Piran, T. 2014, *MNRAS*, 439, 757
- Henden, A. A., Welch, D. L., Terrell, D., & Levine, S. E. 2009, in *American Astronomical Society Meeting Abstracts*, Vol. 214, American Astronomical Society Meeting Abstracts #214, 669
- Hosseinzadeh, G., Arcavi, I., Zalzman, D., et al. 2017, *GCN Circ.*, 21860
- Hotokezaka, K., Kiuchi, K., Kyutoku, K., et al. 2013, *PhRvD*, 87, 024001
- Jin, Z.-P., Hotokezaka, K., Li, X., et al. 2016, *Nature Communications*, 7, 12898
- Kasen, D., Badnell, N. R., & Barnes, J. 2013, *ApJ*, 774, 25
- Kasen, D., Fernández, R., & Metzger, B. D. 2015, *MNRAS*, 450, 1777
- Kulkarni, S. R. 2005, *ArXiv Astrophysics e-prints*, astro-ph/0510256
- Li, L.-X., & Paczyński, B. 1998, *ApJL*, 507, L59
- LIGO Scientific Collaboration, & Virgo Collaboration. 2017a, *Physical Review Letters*, accepted
- . 2017b, *Physical Review Letters*, accepted
- . 2017c, *ApJL*, accepted
- . 2017d, *GCN Circ.*, 21474
- . 2017e, *GCN Circ.*, 21493
- . 2017f, *GCN Circ.*, 21505
- LIGO Scientific Collaboration, Aasi, J., Abbott, B. P., et al. 2015, *Classical and Quantum Gravity*, 32, 074001
- Makarov, D., Prugniel, P., Terekhova, N., Courtois, H., & Vauglin, I. 2014, *A&A*, 570, A13
- McCully, C., Hiramatsu, D., Howell, D. A., et al. 2017, *ApJL*, accepted
- Metzger, B. D. 2017, *Living Reviews in Relativity*, 20, 3
- Metzger, B. D., Bauswein, A., Goriely, S., & Kasen, D. 2015, *MNRAS*, 446, 1115
- Metzger, B. D., & Berger, E. 2012, *ApJ*, 746, 48
- Metzger, B. D., & Piro, A. L. 2014, *MNRAS*, 439, 3916
- Metzger, B. D., Piro, A. L., & Quataert, E. 2008, *MNRAS*, 390, 781
- Metzger, B. D., Martínez-Pinedo, G., Darbha, S., et al. 2010, *MNRAS*, 406, 2650
- Narayan, R., Paczynski, B., & Piran, T. 1992, *ApJL*, 395, L83

- Perley, D. A., Metzger, B. D., Granot, J., et al. 2009, *ApJ*, 696, 1871
- Roberts, L. F., Kasen, D., Lee, W. H., & Ramirez-Ruiz, E. 2011, *ApJL*, 736, L21
- Rosswog, S. 2005, *ApJ*, 634, 1202
- Rosswog, S., Liebendörfer, M., Thielemann, F.-K., et al. 1999, *A&A*, 341, 499
- Rosswog, S., Piran, T., & Nakar, E. 2013, *MNRAS*, 430, 2585
- Schechter, P. 1976, *ApJ*, 203, 297
- Seaman, R., Williams, R., Allan, A., et al. 2011, *Sky Event Reporting Metadata Version 2.0*, IVOA Recommendation 11 July 2011, , , [arXiv:1110.0523](#)
- Sekiguchi, Y., Kiuchi, K., Kyutoku, K., Shibata, M., & Taniguchi, K. 2016, *PhRvD*, 93, 124046
- Singer, L. P., & Price, L. R. 2016, *PhRvD*, 93, 024013
- Singer, L. P., Chen, H.-Y., Holz, D. E., et al. 2016, *ApJL*, 829, L15
- Skrutskie, M. F., Cutri, R. M., Stiening, R., et al. 2006, *AJ*, 131, 1163
- Tanaka, M. 2016, *Advances in Astronomy*, 2016, 634197
- Tanaka, M., & Hotokezaka, K. 2013, *ApJ*, 775, 113
- Tanvir, N. R., Levan, A. J., Fruchter, A. S., et al. 2013, *Nature*, 500, 547
- Valenti, S., Howell, D. A., Stritzinger, M. D., et al. 2016, *MNRAS*, 459, 3939
- White, D. J., Daw, E. J., & Dhillon, V. S. 2011, *Classical and Quantum Gravity*, 28, 085016
- Wollaeger, R. T., Korobkin, O., Fontes, C. J., et al. 2017, *ArXiv e-prints*, [arXiv:1705.07084](#)
- Yang, B., Jin, Z.-P., Li, X., et al. 2015, *Nature Communications*, 6, 7323